JETS AND KINEMATICS IN HADRONIC COLLISIONS

ANDREW R. BADEN

Physics Department, University of Maryland,
College Park, MD 20742, USA

Analysis of colliding-beam hadron experiments ($p + \overline{p} \to X$ and $p + p \to X$) often depend upon observation of "jets" - a highly collimated spray of particles such as π,K,e,μ, and γs forming clusters of energy deposition in calorimeters. In this paper we outline how to define jets from such clusters and discuss the meaning of jet quantities such as transverse energy and mass. Data from the DØ experiment are used to illustrate these concepts. In addition, we review the motivations for using certain optimal coordinates for describing energy-momentum 4-vectors, and derive interesting relationships among the kinematic variables.

1. Kinematics of Hadron Collider Events

To motivate some of the kinematic quantities traditionally used to describe $p\overline{p}$ experiments, one must first recognize that the center-of-mass energy $(\sqrt{s})$ of the scattering in these experiments centers is not fixed. This is a direct consequence of the proton substructure [1], where the scattering constituents are quarks and gluons that reside inside the nucleons, with each parton carrying a fraction x of the total nucleon energy. Scattering of partons of different energy results in a center-of-momentum that does not necessarily coincide with the laboratory frame. A lack of knowledge of the center-of-mass energy guides the choice of kinematic variables.

1.1. *Phase Space Volume*

We start with the definition of a relativistically invariant phase space volume $d\tau$ for an object of momentum $\vec{p}$ and energy E. For a fixed particle mass, $d\tau$ can be written as (see [2]):

$$d\tau \equiv \frac{d^3p}{E} = \frac{dp_x\,dp_y\,dp_z}{E}. \tag{1}$$

Defining z as the $p\overline{p}$ collision axis, we see that of the 4-momentum coordinates p_x, p_y, p_z, and E, only the first two are invariant with respect to a Lorentz transformation from the lab frame along the $\hat{z}$ direction, by virtue of their direction being normal to that of the boost. In addition, we see that even though the coordinates p and θ are not invariant with respect to boosts along $\hat{z}$, invariance will be preserved in the product $p\cos\phi\sin\theta$, which is p_x.

A choice of momentum coordinates which more explicitly reflect the Lorentz invariance of the phase space element is (p_T, y, ϕ, m), where p_T is the momentum transverse to $\hat{z}$ direction, ϕ is the azimuthal angle about $\hat{z}$, m is the mass, and y is the "rapidity" along the $\hat{z}$ direction, defined as

$$y \equiv \frac{1}{2}\ln\frac{E+p_z}{E-p_z} = \frac{1}{2}\ln\frac{1+\beta\cos\theta}{1-\beta\cos\theta} \tag{2}$$

or, equivalently,

$$\beta\cos\theta = \tanh y, \tag{3}$$

where $\beta = p/E$, and θ is, as above, the polar production angle relative to the $\hat{\mathbf{z}}$ axis. For a boost along the $\hat{z}$ direction with some $\beta = \beta_b$, a transformation from the lab frame to the new frame will change the rapidity as follows:

$$y \rightarrow y + y_b$$

where

$$y_b = \ln[\gamma_b(1+\beta_b)]$$

Because $\cos\theta = 1$ for boosts along $\hat{\mathbf{z}}$, it follows that

$$\beta_b = \tanh y_b.$$

The advantage of using the above set of coordinates is clear: the effect of a boost along the z-axis changes only y, and that by only an additive constant.

To calculate $d\tau$ in these coordinates, we first differentiate Eq. (2):

$$dy = dp_z\left(\frac{\partial y}{\partial p_z} + \frac{\partial y}{\partial E}\frac{\partial E}{\partial p_z}\right)$$
$$= dp_z\left(\frac{E}{E^2-p_z^2} - \frac{p_z}{E^2-p_z^2}\frac{p_z}{E}\right)$$

which simplifies to

$$dy = \frac{dp_z}{E}.$$

The components dp_x and dp_y are related to the elements dp_T and $d\phi$ via a transformation from cartesian to polar coordinates in 2 dimensions:

$$dp_x\,dp_y = p_T\,dp_T\,d\phi = \frac{1}{2}dp_T^2\,d\phi.$$

We can now write the volume element $d\tau$ as

$$d\tau = \frac{1}{2}dp_T^2\,dy\,d\phi.$$

Thus particles produced in processes that have a matrix element that varies slowly with rapidity (y) should be distributed uniformly in y. This is the origin of the "rapidity plateau" for single-particle production in hadronic collisions.[3]

Our chosen set of kinematic coordinates is well suited to the analysis of physics issues, and is used extensively to describe the results of measurements in high energy physics. In the following sub-sections, we develop formulae and relationships among p_T, ϕ, y, and m and other quantities of interest.

1.2. *Transverse Energy* ($\mathbf{E_T}$) *and Momentum* ($\mathbf{p_T}$)

One can define the "transverse energy" E_T of a particle as its energy in the rest frame where its $p_z = 0$. Because this quantity is invariant to boosts along $\hat{z}$, we can write in general:

$$E_T^2 \equiv p_x^2 + p_y^2 + m^2 = p_T^2 + m^2 = E^2 - p_z^2 \qquad (4)$$

From Eq. (2) we can solve for p_z, yielding:

$$p_z = E \tanh y \qquad (5)$$

Combining the above two equations gives:

$$
\begin{aligned}
E_T^2 &= E^2 - E^2 \tanh^2 y \\
&= E^2 (1 - \tanh^2 y) \\
&= E^2 / \cosh^2 y
\end{aligned}
$$

or equivalently

$$E = E_T \cosh y. \qquad (6)$$

Note that the p_T is always defined in terms of the 3-momentum $\vec{p}$ as

$$p_T \equiv p \sin \theta. \qquad (7)$$

We wish to stress that these two relativistically invariant quantities (E_T and p_T) are *not* defined in the same way (that is, $E_T \neq E \sin \theta$). More on this below.

Combining Eq. (5) and (6) gives

$$p_z = E_T \sinh y \qquad (8)$$

1.3. *Invariant Mass*

The invariant mass of two particles is defined as

$$
\begin{aligned}
M_{12}^2 &\equiv (p_1^\mu + p_2^\mu)(p_{1\mu} + p_{2\mu}) \\
&= m_1^2 + m_2^2 + 2(E_1 E_2 - \vec{p}_1 \cdot \vec{p}_2)
\end{aligned} \qquad (9)
$$

Using the (p_T, ϕ, y and m) variables, and applying equations from the proceeding sections, we calculate

$$E_1 E_2 = E_{T1} \cosh y_1 E_{T2} \cosh y_2.$$

and

$$
\begin{aligned}
\vec{p}_1 \cdot \vec{p}_2 &= p_{x1} p_{x1} + p_{y1} p_{y1} + p_{z1} p_{z1} \\
&= p_{T1} \cos \phi_1 p_{T2} \cos \phi_2 + p_{T1} \sin \phi_1 p_{T2} \sin \phi_2 + p_{z1} p_{z2} \\
&= p_{T1} p_{T2} \cos \delta\phi + p_{z1} p_{z2} \\
&= p_{T1} p_{T2} \cos \delta\phi + E_{T1} \sinh y_1 E_{T2} \sinh y_2 \\
&= E_{T1} E_{T2} (\beta_{T1} \beta_{T2} \cos \delta\phi + \sinh y_1 \sinh y_2).
\end{aligned}
$$

where $\beta_T \equiv p_T / E_T = \beta \sin \theta \cosh y$, and $\delta\phi \equiv \phi_1 - \phi_2$.

Combining the above results gives

$$M_{12}^2 = m_1^2 + m_2^2 + 2E_{t1}E_{t2}(\cosh \delta y - \beta_{t1}\beta_{t2} \cos \delta \phi), \tag{10}$$

where $\delta y \equiv y_1 - y_2$ and $\cosh \delta y = \cosh y_1 \cosh y_2 + \sinh y_1 \sinh y_2$. We will discuss the consequences of Eq. (10) in the limit $\beta \to 1$ in a subsequent section.

1.4. *Pseudo-Rapidity*

In order to determine the rapidity of a particle, one needs both its $\cos \theta$ and velocity β. Since the velocity requires measuring both E and the mass m, this precludes using a single detector component to measure rapidity. However, in the limit of $\beta \to 1$ (or $m \ll p_T$), Eq. (3) becomes $\cos \theta = \tanh y$, which often provides an excellent approximation to use for the rapidity. We therefore define the "pseudo-rapidity" η as the rapidity of a particle with zero mass (or $\beta = 1$): $\eta \equiv y|_{m=0}$. Using Eq. (2) for y, and setting $\beta = 1$, one obtains

$$\eta \equiv \frac{1}{2} \ln \frac{1 + \cos \theta}{1 - \cos \theta} = -\ln \tan \frac{\theta}{2}. \tag{11}$$

and the inverse equation, which is often useful

$$\cos \theta = \tanh \eta. \tag{12}$$

Eliminating $\cos \theta$ from Eqs. (2) and (11) we have the relationship

$$\tanh y = \beta \tanh \eta. \tag{13}$$

This last equation shows clearly that in the limit $m \to 0$ or $\beta \to 1$, we have $\eta = y$. The pseudo-rapidity η, defined to be independent of β, is therefore another way to measure the location of a particle, equivalent to measuring its polar angle θ. In addition, we can use Eq. (12) to derive the transformation

$$d\theta = -\sin \theta d\eta = -d\eta / \cosh \eta. \tag{14}$$

Since β is always ≤ 1 and the function $\tanh(x)$ is monotonic, the pseudo-rapidity $|\eta|$ of a particle of given p_T is *larger* than its true rapidity $|y|$. Figure 1 shows the difference between η and y as a function of η for protons, for several choices of constant p_T, and Figure 2 shows a similar plot for pions. In each plot, a dashed line is drawn at constant $|\eta| - |y| = 0.1$, corresponding to the size of the calorimeter readout pad at DØ[4]. Rapidity and pseudo-rapidity are equal to within 0.1 for pion p_T of ≥ 0.3 GeV/c, and proton p_T of ≥ 2.0 GeV/c, for all η. This means that one can use η in place of y in kinematic calculations involving pions and protons in this range of p_T values.

It is important to recall that, for *fixed* p_T, the velocity β is a function of pseudo-rapidity η. To see the explicit form, we start with $\beta = p/E$, $E = \sqrt{p^2 + m^2}$, use Eq. (7) for p_T, and Eq. (12) to relate η to θ, to get

$$\beta = \frac{p_T}{\sqrt{E_T^2 - m^2 \tanh \eta^2}} \tag{15}$$

which gives

$$\tanh y = \frac{p_T \tanh \eta}{\sqrt{E_T^2 - m^2 \tanh^2 \eta}}.$$

Given the fact that $|\eta| \geq |y|$, we would expect that for fixed p_T, any single-particle spectrum that is independent of y ($d\sigma/dy$ is constant) would become depleted in the central region when plotting as a function of η. This type of effect would be especially large for particles with low p_T and significant mass:
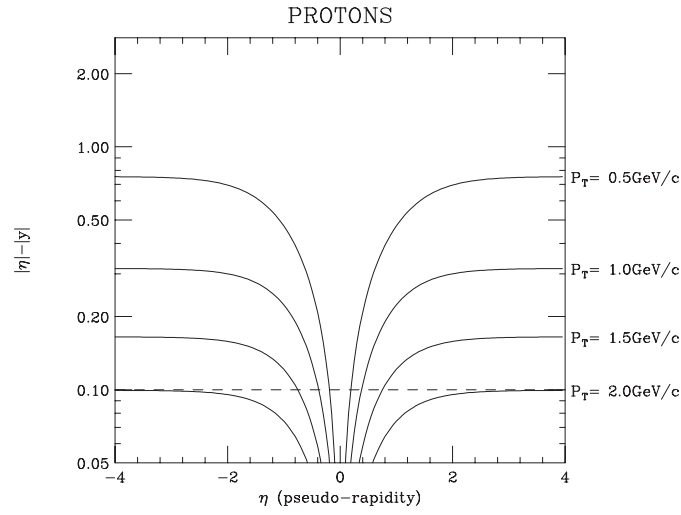
PROTONS

$|\eta|-|y|$

η (pseudo-rapidity)

$P_T = 0.5\,\text{GeV/c}$

$P_T = 1.0\,\text{GeV/c}$

$P_T = 1.5\,\text{GeV/c}$

$P_T = 2.0\,\text{GeV/c}$

Fig. 1. $|\eta| - |y|$ for protons at various p_T.

PIONS

$|\eta|-|y|$

η (pseudo-rapidity)

$P_T = 0.1\,\text{GeV/c}$
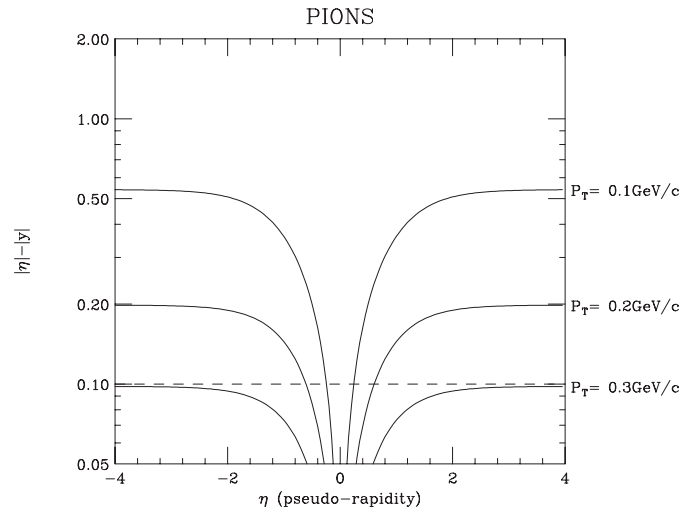
$P_T = 0.2\,\text{GeV/c}$

$P_T = 0.3\,\text{GeV/c}$

Fig. 2. $|\eta| - |y|$ for pions at various p_T.

$$\frac{d\sigma}{d\eta} = \frac{d\sigma}{dy} \cdot \frac{dy}{d\eta} = k \cdot \frac{dy}{d\eta},$$

where k is a constant. An analytic form for $dy/d\eta$ can be derived starting with Eq. 13, substituting for β using Eq. (15), differentiating and rearranging terms to get the result that

$$\frac{dy}{d\eta} = \beta(\eta) \tag{16}$$

with $\beta(\eta)$ given by Eq. (15). This result, although somewhat surprising, can be understood in the following sense: at large y (and therefore large η), the function $\tanh y$ converges to 1. Hence, for large y, both the $\tanh y$ and $\tanh \eta$ converge to 1, which means $\beta \sim 1$ (which would be true for large p and fixed p_T). In this case, there is little if any functional dependence of y on η. At small y, we can use the approximation $\tanh y \sim y$ and $\tanh \eta \sim \eta$ to get the relation $y = \beta\eta$, which gives $dy/d\eta = \beta$. We therefore expect $dy/d\eta$ to be constant for large y or η ($\beta = 1$), with all of the η dependence coming at small η.

Figure 3 shows a histogram of $dN/d\eta$ for 10^6 pions generated with constant $p_T = 0.5$ GeV/c and uniformly in dN/dy. The smooth curve is the function $\beta(\eta)$, that is $dy/d\eta$ for pions with fixed $p_T = 0.5$ GeV/c.
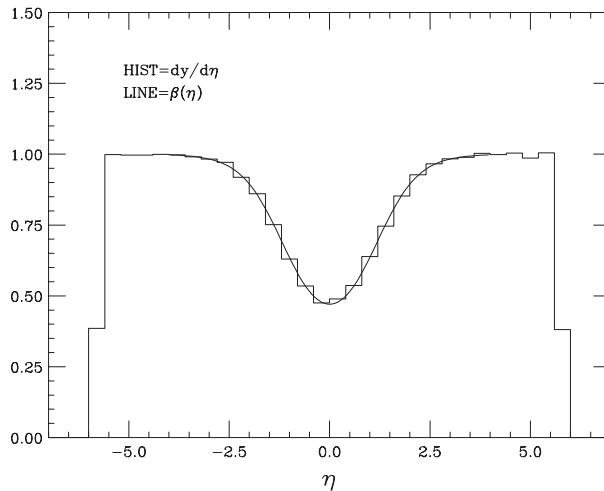

Fig. 3. The histogram shows $dy/d\eta$ for pions generated uniformly in rapidity y, with fixed $p_T = 0.5$ GeV/c. The smooth curve is the corresponding function $\beta(\eta)$.

1.5. *Invariant Masses for $\beta = 1$*

In the limit $m \to 0$, $y \to \eta$ and $\beta = \beta_T \to 1$. We can then write the invariant mass of two massless particles (using Eq. (10)) as:

$$M_{12}^2 = 2E_{T1}E_{T2}(\cosh \delta\eta - \cos \delta\phi). \tag{17}$$

This expression is often quite useful, as we show below.

1.6. *Transverse Mass and "Missing" Transverse Energy*

Non-interacting particles such as neutrinos can be detected only via an apparent imbalance of momentum in an event. In $p\bar{p}$ (or pp) interactions, where most of the longitudinal (parallel to the beam $-\hat{\mathbf{z}}$) momentum in the collision is lost down the beam pipe, it is essentially impossible to measure momentum conservation along $\hat{\mathbf{z}}$. However, given a detector with sufficiently large acceptance, measuring momentum balance in the plane *transverse* to the beam direction is relatively straightforward. Thus, that amount of transverse momentum required to satisfy momentum conservation (the "missing" transverse momentum) can be in large part attributed to the presence of any unobserved non-interacting particles, especially when the total momentum (and energy) in the detector is large (since for small total detected energy, small fluctuations in the measured momentum along any given direction can give a small, statistically insignificant, missing transverse momentum). Since the neutrino is massless (certainly on these scales), this quantity (missing transverse momentum) is virtually equivalent to the *missing transverse energy* (or $\not{E}_T$) in the event.

For particles such as the W boson, which decay into lepton–neutrino pairs, the lack of a measurement of p_z for the neutrino precludes a direct measurement of the invariant mass of the W. However, one can calculate an invariant *transverse mass* of these two particles (denoted by M_T), defined as the invariant 2-particle mass using only the momentum components in the transverse plane (p_{xi} and p_{yi}, i=1,2). From this definition, the transverse mass is defined as

$$M_T^2 \equiv (p_{T1}^\mu + p_{T2}^\mu)(p_{\mu T1} + p_{\mu T2}),$$

where $p_{Ti}^\mu = (E_{Ti}, \vec{\mathbf{p}}_{Ti})$. For two zero-mass particles, ($E_{Ti} = p_{Ti}$) we have

$$
\begin{aligned}
M_T^2 &= 2(E_{T1}E_{T2} - \vec{\mathbf{p}}_{T1} \cdot \vec{\mathbf{p}}_{T2}) \\
&= 2E_{T1}E_{T2}(1 - \cos\delta\phi) \\
&= 4E_{T1}E_{T2}\sin^2(\frac{\delta\phi}{2}).
\end{aligned}
\tag{18}
$$

or, equivalently,

$$M_T = 2\sin(\frac{\delta\phi}{2})\sqrt{E_{T1}E_{T2}}. \tag{19}$$

We can see that this formula is equivalent to Eq. (17) with the condition $\eta_1 = \eta_2$, that is the transverse mass and the invariant mass are equivalent for particles which are produced at the same rapidity ($\delta\eta = 0$). As such, $M_T \leq M_{12}$ (ignoring the detector resolution and intrinsic width Γ_W). As a rule, M_T will deviate from M_{12} as $\delta\eta$ gets large, that is as the particles decay more "forward-backward" in the lab frame. Distributions in M_T will therefore have a tail at low M_T (forward-backward), will peak at M_{12}, and will fall to zero above M_{12} in the same manner as M_{12}.

It is important to note that these formulae require that E_T be defined using Eq. (4) and <u>not</u> as $E\sin\theta$. They are equivalent only in the limit $m/p_T \to 0$. Of course, Eq. (7) is true in general. As will be shown below, in the small mass limit of $\beta \to 1$, the difference between E_T and p_T becomes insignificant.

An interesting relationship involving the invariant mass of 3 particles is

$$M_{123}^2 = M_{12}^2 + M_{23}^2 + M_{13}^2 - m_1^2 - m_2^2 - m_3^2$$

which in the limit of $m_i \to 0$ becomes

$$M_{123}^2 = M_{12}^2 + M_{23}^2 + M_{13}^2. \tag{20}$$

This formula is interesting to keep in mind when searching for 3-body decays, say $A \to a + b + c$. If it is appropriate to ignore the three masses m_a, m_b, and m_c, then you do not have to know which of the three bodies is a, b, or c specifically in order to calculate the correct value for m_A – you only have to know that these *are* the 3 bodies of which you are interested.

Lastly, since the mass of the W particle is well known [5], we can constrain the invariant mass of the e, ν pair, and solve for the longitudinal momentum of the neutrino. To do this, we can use Eq. (17):

$$M_W^2 = 2E_{T1}E_{T2}(\cosh \delta\eta - \cos \delta\phi).$$

Rewriting this expression, we get

$$\cosh \delta\eta = \frac{M_W^2}{2E_{T1}E_{T2}} + \cos \delta\phi. \tag{21}$$

Solving for $\delta\eta$ gives

$$\delta\eta = ln\frac{r + \sqrt{r^2 - 1}}{2}, \tag{22}$$

where r is the right-hand side of Eq. (21). Because $\delta\eta$ is the difference in pseudorapidity between the electron and the neutrino, there are two solutions to the problem. That is, there is no way of resolving the ambiguity of whether the neutrino is at a lower or higher rapidity relative to the electron as seen from the fact that the hyperbolic cosine $\cosh \delta\eta$ is even in $\delta\eta$. Both solutions are possible, at least in principle.

2. Jets

Quantum Chromodynamics (QCD [678]) is the currently accepted theory of the strong interaction between particles (partons) that carry "color". These partons (quarks q and gluons g) appear in detectors as "sprays", or "jets", of particles. In this section, we will discuss issues concerning the observation of jets and their origin in QCD.

2.1. *Definition of a Jet*

There are various ways to define jets. For instance, most of the LEP, PEP, and PETRA e^+e^- experiments define jets using information just from tracking chambers [9]. One of the less ambiguous ways to define jets is motivated by what we understand to be the physics of fragmentation, namely that a jet is the result of the hadronization of a parent parton. A way to visualize hadronization is through virtual gluon emission by the parent parton ($q \to q + g$ and $g \to g + g$), followed by gluon splitting to $q\overline{q}$ pairs, forming the color singlet hadrons that we measure. For high precision studies of parton QCD fragmentation in e^+e^- collisions, this model is too naive. However, in hadronic collisions, where the presence of the soft "underlying event" part of a high Q^2 collision complicates the analysis, the naive model is adequate for describing how a parton turns into a jet.

To see how this simple fragmentation model can be related to the concept of a jet, we consider the transverse momentum (k_T) of (radiated) gluons relative to the jet axis. The distribution of k_T has been found to be exponential in $-k_T^2$, with $\langle k_T \rangle \simeq 300$ MeV/c at SPEAR [10] and DORIS [11] energies ($\sqrt{s} \simeq 10 GeV$), increasing to $\langle k_T \rangle \simeq 1 GeV/c$ at $Sp\overline{p}S$ energies.[12] We define ψ as the angle of the gluon with respect to some reference in the plane perpendicular to the momentum direction of
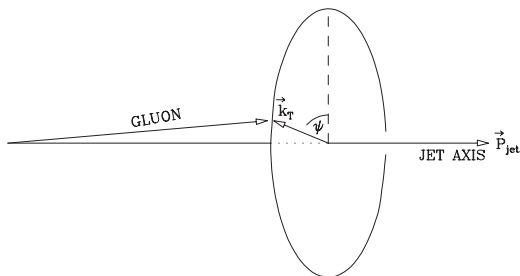
Fig. 4. Radiated gluons make an angle ψ with respect to an arbitrary direction in the plane perpendicular to the jet axis.

the parent parton (see Figure 4). Since the physics of gluon radiation is independent of this angle, we expect the probability distribution for ψ will be uniform in ψ. The jet axis can be defined by a cluster of calorimeter cells (less often by tracks in the tracking chamber) in space that minimize the total vector $\vec{k}_T$ of the jet remnants. This means requiring:

$$\sum \vec{\mathbf{k}}_{Ti} = 0, \qquad (23)$$

We can use Eq. (23) to form the jet cluster into an equivalent particle with 4-momentum $p^\mu = (E, \vec{\mathbf{p}})$, that can be used, for example, to calculate an invariant mass (for example $W \to \mathrm{jet} + \mathrm{jet}$). Let us specialize to calorimetry, and assume that the jet will be constructed as a cluster of cells (or towers for projective geometry calorimeters). If one represents the energy E_i in each cell of a calorimeter i as a "particle" with zero mass, one can then define $\vec{\mathbf{E}}_i = E_i \hat{\mathbf{n}}_i$ where $\hat{\mathbf{n}}_i$ is the unit vector pointing from the interaction vertex to cell i. The jet is therefore defined in the rest frame of the detector as an object consisting of a set of these zero mass particles (and therefore $p_i = E_i$), one per calorimeter cell. Note that this representation of a jet (using zero mass particles) does not imply that the jet also has zero mass, or $p = E$, since the constituents (the cells) will each have an opening angle between them, and this opening angle will "generate" a jet mass. To see this explicitly, consider Eq. (9, the invariant mass of two particles. If the particles have zero mass, we drop the terms m_1 and m_2, set $E_1 = p_1$ and $E_2 = p_2$, leaving

$$M_{12}^2 = 2 E_1 E_2 (1 - \cos\theta) = 4 E_1 E_2 \sin^2\theta,$$

where θ is the angle between the two particles. We see clearly that if $\theta = 0$, the invariant mass is also zero.

To form a jet from these calorimeter cells, we must apply Eq. (23) relative to the axis that defines the jet direction. The transformation of the cells to this axis involves an Euler rotation with 2 degrees of freedom: ϕ_{jet} and θ_{jet}. The rotation matrix $\mathbf{M}$, defined by $\vec{E}'_i = M\vec{E}_i$, is a function of the yet to be determined Euler angles, and is given by [13]

$$\begin{pmatrix} -\sin\phi_{jet} & \cos\phi_{jet} & 0 \\ -\cos\theta_{jet}\cos\phi_{jet} & -\cos\theta_{jet}\sin\phi_{jet} & \sin\theta_{jet} \\ \sin\theta_{jet}\cos\phi_{jet} & \sin\theta_{jet}\sin\phi_{jet} & \cos\theta_{jet} \end{pmatrix}$$

The transformation equations which relate the cell energies in the frame of the jet (primed) to those in the frame of the detector (unprimed) are therefore

$$\begin{aligned} E'_{xi} &= -E_{xi}\sin\phi_{jet} + E_{yi}\cos\phi_{jet} \\ &= E_{Ti}\sin\delta\phi_i \\ E'_{yi} &= -E_{xi}\cos\theta_{jet}\cos\phi_{jet} - E_{yi}\cos\theta_{jet}\sin\phi_{jet} + E_{zi}\sin\theta_{jet} \\ &= -\cos\theta_{jet}E_{Ti}\cos\delta\phi_i + \sin\theta_{jet}E_{zi} \\ E'_{zi} &= E_{xi}\sin\theta_{jet}\cos\phi_{jet} + E_{yi}\sin\theta_{jet}\sin\phi_{jet} + E_{zi}\cos\theta_{jet} \\ &= \sin\theta_{jet}E_{Ti}\cos\delta\phi_i + \cos\theta_{jet}E_{zi}, \end{aligned} \tag{24}$$

where $E_{Ti} = E_i\sin\theta_i$, and $\delta\phi_i \equiv \phi_i - \phi_{jet}$. As a check of Eq. (24), we can imagine a jet with a single tower which when rotated to the jet axis should retrieve $E'_x = E'_y = 0$ and $E'_z = E_{jet}$. Thus, setting $\delta\phi = 0$ (remember that $\delta\phi$ is the difference in ϕ between the jet and the tower), the above equations yield $E'_x = 0$, $E'_y = E_z\sin\theta_{jet} - E_T\cos\theta_{jet} = 0$ (using $\tan\theta_{jet} = E_T/E_z$), and $E'_z = E_T\sin\theta_{jet} + E_z\cos\theta_{jet} = E_{jet}$ (using $E_T = E\sin\theta_{jet}$ and $E_z = E\cos\theta_{jet}$). Here we have assumed that such a hypothetical jet would be massless since it is contained in a single tower, allowing $E_{jet} = p_{jet}$ in the above. This is discussed further below.

The momentum vectors of each tower can now be rotated into the frame of the jet, summed over the transverse components $E'_{xi} \equiv k_{xi}$ and $E'_{yi} \equiv k_{yi}$, and separately set to zero, as required by Eq. (23):

$$\sum_i E'_{xi} = -\sin\phi_{jet} \cdot \sum_i E_{xi} + \cos\phi_{jet} \cdot \sum_i E_{yi} = 0 \tag{25}$$

and

$$\begin{aligned} \sum_i E'_{yi} &= -\cos\theta_{jet}\cos_{jet}\phi \cdot \sum_i E_{xi} - \\ &\quad \cos\theta_{jet}\sin\phi_{jet} \cdot \sum_i E_{yi} + \sin\theta_{jet} \cdot \sum_i E_{zi} \\ &= 0. \end{aligned} \tag{26}$$

We therefore have two equations (25 and 26) and two unknowns (ϕ_{jet} and θ_{jet}). Solving Eq. (25) yields the following relation:

$$\tan\phi_{jet} = \frac{\sum E_{yi}}{\sum E_{xi}} = \frac{\sum E_{Ti}\sin\phi_i}{\sum E_{Ti}\cos\phi_i}. \tag{27}$$

Solving Eq. (26) gives

$$\tan\theta_{jet} \;=\; \frac{\cos\phi_{jet}\cdot\sum_i E_{xi} + \sin\phi_{jet}\cdot\sum_i E_{yi}}{\sum_i E_{zi}}. \tag{28}$$

Equations (27) and (28) describe the coordinates of the jet cluster in a way which is consistent with the defining Eq. (23).

The jet is a true physical object, which might have originated through the showering of some virtual parton, and it must therefore have a 4-vector $(E_{jet}, \vec{\mathbf{p}}_{jet})$ that corresponds to an object of some finite mass. We can define the angles of our jet in the laboratory, as follows:

$$\tan\phi_{jet} = \frac{p_{yjet}}{p_{xjet}} \tag{29}$$

and

$$\tan\theta_{jet} = \frac{p_{tjet}}{p_{zjet}} \tag{30}$$

or equivalently, using the relation that $\sinh\eta\tan\theta = 1$,

$$\sinh\eta_{jet} \;=\; \frac{p_{zjet}}{p_{tjet}}. \tag{31}$$

Equating the numerators and denominators of Eqs. (27)and (29), we obtain the result:

$$
\begin{aligned}
p_{xjet} \;&\equiv\; \sum_{i=1}^{\#towers} E_{xi} \\
&=\; \sum_{i=1}^{\#towers} E_i \sin\theta_i \cos\phi_i \\
&=\; \sum_{i=1}^{\#towers} E_{Ti} \cos\phi_i.
\end{aligned} \tag{32}
$$

and

$$
\begin{aligned}
p_{yjet} \;&\equiv\; \sum_{i=1}^{\#towers} E_{yi} \\
&=\; \sum_{i=1}^{\#towers} E_i \sin\theta_i \sin\phi_i \\
&=\; \sum_{i=1}^{\#towers} E_{Ti} \sin\phi_i.
\end{aligned} \tag{33}
$$

By comparing the numerators and denominators of Eqs. (28) and (30), we get

$$
\begin{aligned}
p_{zjet} \;\equiv\; & \sum_{i=1}^{\#towers} E_{zi} \\
= \; & \sum_{i=1}^{\#towers} E_i \cos\theta_i \\
= \; & \sum_{i=1}^{\#towers} E_i \tanh\eta_i \\
= \; & \sum_{i=1}^{\#towers} E_{Ti} \sinh\eta_i,
\end{aligned}
\tag{34}
$$

where we have again used the relationship $\sinh\eta\tan\theta = 1$, and not shown the details of the algebra. We have also used the fact that, for the towers, $E_{Ti} \equiv E_i \sin\theta_i$ remembering that in our approximation each calorimeter tower be represented as a particle of zero mass.

It should be recognized that the coordinate θ_{jet} was derived from Eq. (28), and the coordinate η_{jet} from Eq. (31), using the relationship $\eta = -\log\tan\theta/2$. Consequently, the true η does *not* correspond to the energy weighted result $\eta_{jet} = \sum E_{Ti}\eta_i / \sum E_{Ti}$.

The energy of the jet is given by an energy sum over all towers in the cluster:

$$
E_{jet} \equiv \sum_{i=1}^{\#towers} E_i.
\tag{35}
$$

We have therefore established a self-consistent prescription for turning a "cluster" of energy towers into a physical jet, which is a particle with 4-momentum in the detector frame given by

$$
p_{jet}^{\mu} \;=\; \left(\sum E_i, \sum \vec{\mathbf{p}}_i\right) \;=\; \left(\sum E_i, \sum E_i \hat{\mathbf{n}}_i\right)
\tag{36}
$$

and with directional coordinates θ_{jet} (or η_{jet}) and ϕ_{jet} derived from the above momentum components, or as calculated using Eq. (32) through (34).

It is worth investigating expressions for the jet 4-vector that involve not just sums over towers at specific angles η_i and ϕ_i, but rather sums that involve angles relative to the jet axis: $\delta\eta_i \equiv \eta_{jet} - \eta_i$ and $\delta\phi_i \equiv \phi_{jet} - \phi_i$.

The expression for p_{Tjet} is straightforward. We use the numerator of Eq. (28):

$$
p_{Tjet} = \cos\phi_{jet} \cdot \sum_i E_{xi} + \sin\phi_{jet} \cdot \sum_i E_{yi}
$$

and substitute in $E_{xi} = E_{Ti}\cos\phi_i$ and $E_{yi} = E_{Ti}\sin\phi_i$. This gives

$$
\begin{aligned}
p_{Tjet} \;=\; & \cos\phi_{jet} \cdot \sum_i E_{Ti}\cos\phi_i + \sin_{jet}\phi \cdot \sum_i E_{Ti}\sin\phi_i \\
= \; & \sum_i E_{Ti}\cos\delta\phi_i
\end{aligned}
\tag{37}
$$

The expression for E_{Tjet} is not as straightforward. First, we form $E_T^2 \equiv E^2 - p_z^2$ and use the relation $\cosh^2 x - \sinh^2 x = 1$ to get

$$
\begin{aligned}
E_{Tjet}^2 &= E_{jet}^2 - p_{zjet}^2 \\
&= E_{jet}^2(\cosh\eta_{jet}^2 - \sinh\eta_{jet}^2) - p_{zjet}^2(\cosh\eta_{jet}^2 - \sinh\eta_{jet}^2) \\
&= (E_{jet}^2\cosh\eta_{jet}^2 + p_{zjet}^2\sinh\eta_{jet}^2) - (E_{jet}^2\sinh\eta_{jet}^2 + p_{zjet}^2\cosh\eta_{jet}^2)
\end{aligned}
$$

If we add and subtract the quantity $2E_{jet}p_{zjet}\sinh\eta_{jet}\cosh\eta_{jet}$, and then use Eqs. (35) and (34) in the above equation we get

$$
\begin{aligned}
E_{Tjet}^2 &= (E_{jet}\cosh\eta_{jet} - p_{zjet}\sinh\eta_{jet})^2 + (E\sinh\eta_{jet} - p_{zjet}\cosh\eta_{jet})^2 \\
&= (\sum E_i\cosh\eta_{jet} - \sum E_{zi}\sinh\eta_{jet})^2 + (\sum E_i\sinh\eta_{jet} - \sum E_{zi}\cosh\eta_{jet})^2 \\
&= (\sum E_{Ti}\cosh\eta_i\cosh\eta_{jet} - \sum E_{Ti}\sinh\eta_i\sinh\eta_{jet})^2 + \\
&\quad (\sum E_{Ti}\cosh\eta_i\sinh\eta_{jet} - \sum E_{Ti}\sinh\eta_i\cosh\eta_{jet})^2 \\
&= (\sum E_{Ti}\cosh\delta\eta_i)^2 - (\sum E_{Ti}\sinh\delta\eta_i)^2
\end{aligned}
\tag{38}
$$

This equation is not altogether transparent. However, consider the symmetry of the sinh and cosh functions – the former is odd, the latter is even. If the jet is symmetric (in energy and physical extent) about the jet axis, then the sum over $E_{Ti}\sinh\delta\eta_i$ will vanish, leaving

$$
E_{Tjet} = \sum E_{Ti}\cosh\delta\eta_i
\tag{39}
$$

Eqs. (37) and (39) will prove useful later in our exposition.

2.2. *Jet (or Clustering) Algorithm*

The final missing ingredient is an algorithm for determining which calorimeter cells to include in a cluster that is consistent with Eq. (23). One such scheme, usually referred to as a "fixed-cone" algorithm used by UA1 [14], CDF [15], and DØ[16], works in the following way:

- All towers above a moderate energy threshold serve as "seed towers" for initial "proto-clusters".

- All immediately neighboring towers within some cone cutoff R in $\eta\phi$ space (a common range for the cone cutoff R is 0.3-0.7), relative to the center of the proto-cluster ($R = \sqrt{\delta\eta^2 + \delta\phi^2}$) are added to form a new cluster. The centroids (or 1st moments) of the cluster in η and ϕ are recalculated. These towers may or may note be subject to a small energy threshold.

- If the jet centroid in $\eta\phi$ changes by more than some small preset value, then all towers within the cone R are re-combined to form a new cluster. Again the centroids are calculated in η and ϕ. This procedure is iterated until the centroid of the cluster remains stable.

- After all clusters are found, some may contain overlapping (same) calorimeter towers. If so, such clusters are merged, depending on the fraction of transverse energy present in the shared towers. The smaller E_T cluster is then subsumed.

A threshold parameter controls the merging. For the data to be shown in this report, the merging parameter was set to 0.5 (50% of the energy shared by any two clusters will cause merging).

Another algorithm, called the "nearest-neighbor" algorithm, was the primary clustering algorithm used by UA2, and is described elsewhere. [17]

2.3. *The Shape of a Jet*

Equation (24) can be used to calculate the component of the tower energy (or momentum) that is transverse to the jet direction: $k_{Ti}^2 \equiv E_{xi}'^2 + E_{yi}'^2$. For those towers that are "close" to the jet axis, the small-angle limit of Eq. (24) gives

$$
\begin{aligned}
E_{xi}' &\sim E_{Ti}\delta\phi_i \\
E_{yi}' &\sim \sin\theta_{jet}E_{zi} - \cos\theta_{jet}E_{Ti} \\
&= \sin\theta_{jet}E_i\cos\theta_i - \cos\theta_{jet}E_i\sin\theta_i \\
&= E_i\sin\delta\theta_i \\
&\sim E_i\delta\theta_i \\
&= -E_{Ti}\delta\eta_i
\end{aligned}
$$

where we have used $\delta\theta = -\sin\theta\delta\eta$ from Eq. (14), and the relation $E_{Ti} = E_i\sin\theta_i$. Squaring and adding the components gives

$$
k_{Ti}^2 \simeq E_{Ti}^2(\delta\phi_i^2 + \delta\eta_i^2),
$$

or, equivalently,

$$
k_{Ti} \simeq E_{Ti}R_i \tag{40}
$$

where R_i is the distance between the jet and cell i in $\eta\phi$ space defined by

$$
R_i^2 \equiv \delta\eta_i^2 + \delta\phi_i^2. \tag{41}
$$

Thus, the momentum of each "particle" in the $\eta\phi$ plane is given by the product of the E_T of the particle (in the lab frame) and the distance in $\eta\phi$ space from the jet axis. Since the k_{Ti} are expected to be symmetrically distributed about the jet axis (Figure 4), this suggests that jets have circular shapes in $\eta\phi$ space. Of course, this small angle limit is not a good approximation for "particles" (cells) that are far off the jet axis.

It is best to define the shape of a jet using an energy weighting procedure. This reduces the dependence of the shape on low energy towers that are both far from the jet axis and have a negligible contribution to the total jet energy. The shape of a jet is often characterized by an E_{Ti}-weighted second moment (variance) of the distance in the transverse plane. Since the first moment vanishes:

$$
\sum \vec{\mathbf{k}}_{Ti} = \sum E_{Ti}\vec{\mathbf{R}}_i = 0,
$$

we have

$$
\sigma_R^2 \equiv \frac{\sum E_{Ti}R_i^2}{\sum E_{Ti}} = \frac{\sum E_{Ti}(\delta\phi_i^2 + \delta\eta_i^2)}{\sum E_{Ti}} \tag{42}
$$

which is equivalent to

$$
\sigma_R^2 \equiv \sigma_{\eta\eta} + \sigma_{\phi\phi} \tag{43}
$$

when we define $\sigma_{\eta\eta}$ and $\sigma_{\phi\phi}$ as:

$$\sigma_{\eta\eta} \equiv \frac{\sum E_{Ti}\delta\eta_i^2}{\sum E_{Ti}}, \;\; \sigma_{\phi\phi} \equiv \frac{\sum E_{Ti}\delta\phi_i^2}{\sum E_{Ti}}. \tag{44}$$

Referring to data, for some specific R we first define

$$\sigma_R \equiv \sqrt{\sigma_R^2} = \sqrt{\sigma_{\eta\eta} + \sigma_{\phi\phi}} \tag{45}$$

using events from DØ described in Appendix 1 (Sample 1). This data sample was selected to minimize jet merging (2 to 1), a process that has origin in higher-order QCD effects that are distinct from those of jet fragmentation.

Figure 5 shows the distribution of the second moment σ_R for three jet cone cutoffs of $R = 0.3, 0.5$, and 0.7. The points are DØ data. The effect of the cone cutoff is clear: the larger the cone, the larger the 2nd moment in both mean and width. The main source of the broadening is simply due to the presence of additional towers for the larger cone cutoffs. Figure 5 also shows the results of Gaussian fits to the distributions. The fits reveal that for unmerged jets, the distribution of jet widths is well described by a Gaussian, with a central value that is a function of the cone cutoff. This is not to say that the energy flow around the jet axis has a Gaussian distribution - rather, this is only describing the fluctuations in σ_R (the jet RMS) around the average σ_R, which is itself a function of the jet cone parameter. Table 1 shows the results for the fits, and Figure 6 shows that the central value of

Table 1. Results of a Gaussian fit to distributions of σ_R using the data from Sample 1.

R	$\overline{\sigma_R}$	RMS(σ_R)
0.3	$.132 \pm .002$	$.024 \pm .002$
0.5	$.193 \pm .004$	$.040 \pm .004$
0.7	$.255 \pm .005$	$.054 \pm .005$

the distribution in σ_R (mean of the Gaussian) scales linearly with the cone cutoff .

The small angle approximation used above is clearly excellent. Figure 5 shows that even for jets with $R = 0.7$, $\sigma_R < 0.42$ about 90% of the time. This shows that the above approximation is valid for all but perhaps 1% of the $R = 0.7$ jets (with largest RMS widths).

2.4. *Jet $\eta\phi$ Correlation Matrix*

Detector effects, gluon radiation, and the underlying event, all contribute to distorting the shape of jets. Figure 7 shows a sketch of a typical elliptical "real" jet, with α defined as the smaller of the angles between the semi-major axis and either the η or ϕ axis. The angle α can be calculated from the variance in η and ϕ, as defined in Eq. 44, and from the corresponding correlation term $\sigma_{\eta\phi}$, defined as

$$\sigma_{\eta\phi} \equiv \frac{\sum E_{Ti}\delta\eta_i\delta\phi_i}{\sum E_{Ti}}. \tag{46}$$

The shape of the jet can be characterized by the correlation term $\sigma_{\eta\phi}$ and the "diagonal" terms $\sigma_{\eta\eta}$ and $\sigma_{\phi\phi}$ in the shape matrix:

$$\begin{pmatrix} \sigma_{\eta\eta} & \sigma_{\eta\phi} \\ \sigma_{\eta\phi} & \sigma_{\phi\phi} \end{pmatrix}$$

Upon diagonalization, the two eigenvalues corresponding to the semi–major (σ_+^2) and semi–minor (σ_-^2) axes are
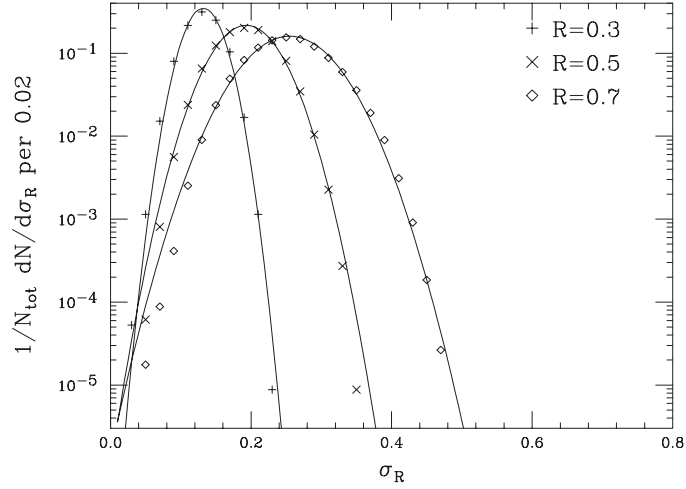
Fig. 5. Jet probability distribution in σ_R for single unmerged jets.
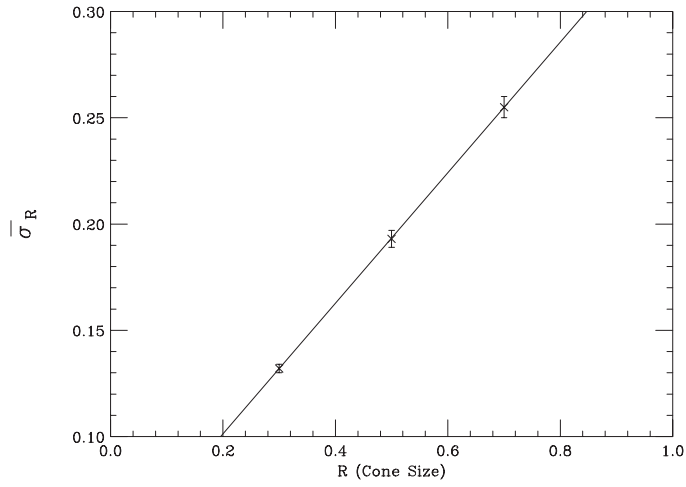

Fig. 6. Results of a Gaussian fit to distributions in σ_R as a function of the cone cutoff R. The straight line is from a linear fit to the points yielding $\overline{\sigma_R} = (0.040 \pm 0.005) + (0.31 \pm 0.01) \cdot R$.
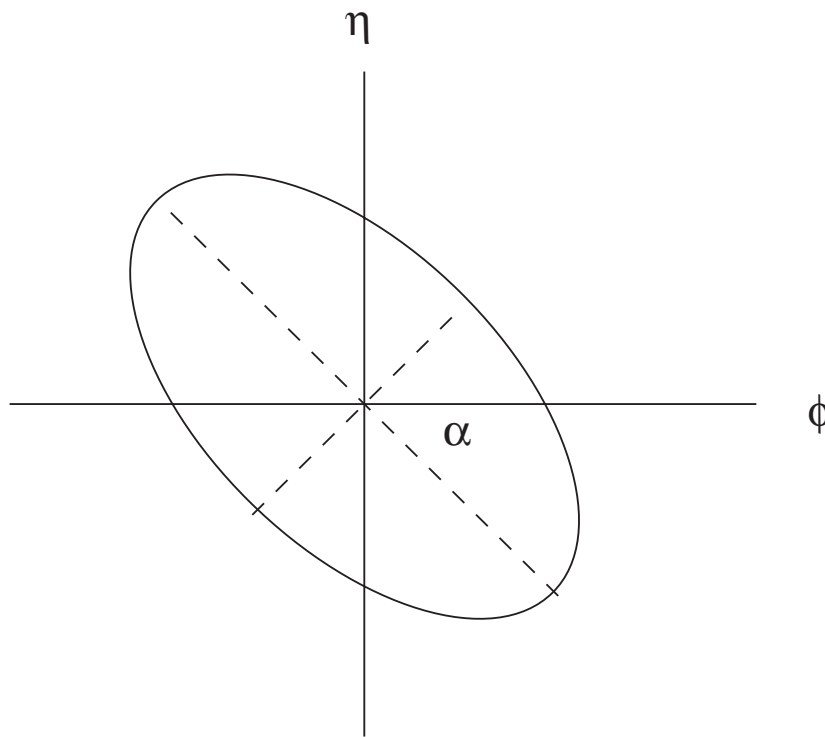
Fig. 7. Jet ellipse. Semi-major and -minor axes represent the square root of the second moment in η ($\sigma_{\eta\eta}$) and ϕ ($\sigma_{\phi\phi}$).

$$\sigma_\pm^2 = \frac{\sigma_{\eta\eta} + \sigma_{\phi\phi}}{2} \pm \sqrt{\left(\frac{\sigma_{\eta\eta} - \sigma_{\phi\phi}}{2}\right)^2 + \sigma_{\eta\phi}^2} \qquad (47)$$

It is clear that for a circular jet ($\sigma_{\eta\phi} = 0$), $\sigma_+^2 = \sigma_{\eta\eta}$ and $\sigma_-^2 = \sigma_{\phi\phi}$.

We now return to Eq. (45), which defined the quantity σ_R, the RMS width of the jet in $\eta\phi$ space. This quantity is of course the square root of the sum of the two diagonal terms of the shape matrix, and not the root of the sum of the squares of these two terms. The off-diagonal term $\sigma_{\eta\phi}$ does not affect σ_R.

2.5. *The* E_T *of a Jet*

A common way for experimenters to characterize the hard scattering energy scale (Q^2) for QCD collisions which produce jets is to use the transverse energy E_T of a produced jet. The measure of E_T which is most often used to compare data to QCD theory is

$$E_T \equiv \sum_{i=1}^{\#towers} E_{Ti}. \qquad (48)$$

It has the advantage that one can hope to establish a correspondence between the energy observed in each tower (experiment) and the particles radiated by a jet (a hadronized parton). There are, however, two other ways to define E_T, one of which is more amenable for treating a jet as a collection of physical objects (particles), and possibly more appropriate for calculating invariant masses involving jets. The first is:

$$E_T \equiv E_{jet} \sin\theta_{jet} \qquad (49)$$

where $\sin\theta_{jet}$ is related to η_{jet} through Eq. (12), and E_{jet} is calculated using Eq. (35). The second way to define E_T uses Eqs. (4) and (36). As long as there is consistency in comparing theory to experiment, it is relatively arbitrary how one defines E_T (given that all internal variables are calculated consistently). However, because of the differences between p_T and E_T, the definition in Eq. (49) should not be used in calculating the invariant mass given in Eq. (17). For such cases, only the E_T defined in Eq. (4) is appropriate.

To see this clearly, we use the relation $E^2 = p^2 + m^2$ and write

$$(E\sin\theta)^2 \; = \; (p^2 + m^2)\sin^2\theta \; = \; p_T^2 + m^2\sin^2\theta.$$

We see that this definition gives a *systematically* lower value for the transverse energy E_T than the relativistically correct definition from Eq. (4). The difference, of course, is insignificant in the high energy limit (jet velocity $\beta \sim 1$), and for jets that are produced at $90°$ ($\eta = 0$) to the beam axis (so-called "central jets").

We can quantify the difference in the two definitions of E_T through the quantity:

$$\Delta \equiv 1 - \frac{E\sin\theta}{E_T} = 1 - \frac{\sqrt{p_T^2 + m^2\sin^2\theta}}{\sqrt{p_T^2 + m^2}}. \qquad (50)$$

which measures the fractional "error" in using Eq. (49). Expanding Eq. (50) for small mass, and keeping only the lowest powers of m^2/p_T^2, gives

$$\Delta = \frac{m^2\tanh^2\eta}{2p_T^2}. \qquad (51)$$

This shows the explicit dependence of the difference (Δ) on p_T (for arbitrary values of η). For small η, $\tanh^2 \eta \simeq \eta^2$ and Δ rapidly approaches zero. Coupled with the fact that $m < E_T$, for all but the smallest-E_T jets, we conclude that, typically, Eq. (49) and Eq. (4) agree at the few percent level for $\eta < 0.5$.

Figure 8 shows the distribution in Δ for the highest-E_T jet in 2-jet events from our Sample 1 (Appendix 1). Figure 9 shows the integrated probability as a function of a lower cutoff on Δ (the percentage of jets that would be mismeasured, if Δ were greater than the value given on the abscissa). The distributions clearly broaden with jet cone size. Because Δ is proportional to m^2, the broadening can be attributed to the broadening of the mass of a jet due to the increase in the number of jet towers with the cone size (including towers that might not "belong" in the jet). Such broadening can also come about from the failure to merge two jets into one, where one of the two jets might have an energy below an E_T threshold. (Such a threshold is usually employed by the experiments to eliminate the number of jets found at very low energy.)
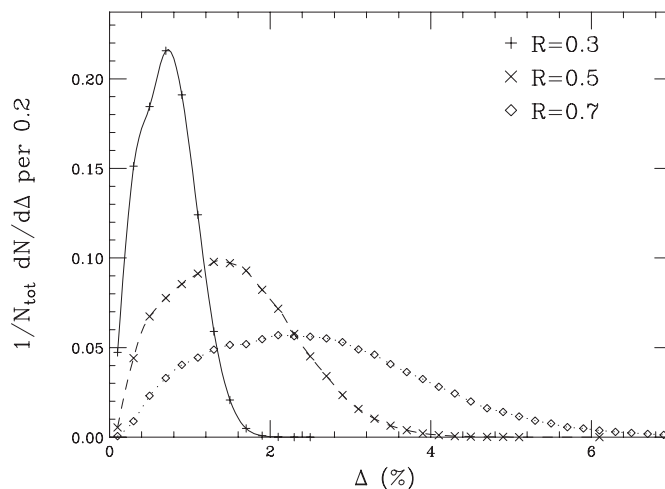

Fig. 8. Distribution in Δ as defined using Eq. (50) for jets of Sample 1, required to have $|\eta| \geq 0.5$.

The E_T defined in Eq. (48) also underestimates the true E_T of the jet (as defined using Eq. 4). This can be seen as follows. Suppose there is a cluster with just 2 towers, then Eq. (4) would yield

$$
\begin{aligned}
E^2 - p_z^2 &\equiv (E_1 + E_2)^2 - (p_{z1} + p_{z2})^2 \\
&= (E_1 + E_2)^2 - (E_1 \cos\theta_1 + E_2 \cos\theta_2)^2 \\
&= E_{T1}^2 + E_{T2}^2 + 2E_1 E_2(1 - \cos\theta_1 \cos\theta_2)
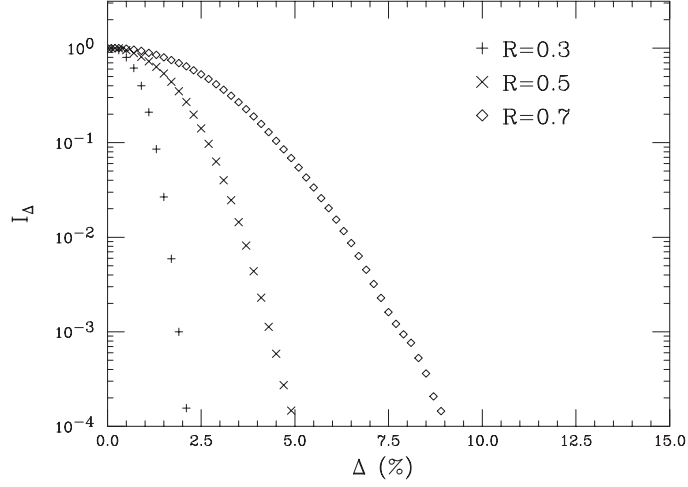\end{aligned}
$$

(52)

while equation (48) would yield

Fig. 9. $I_\Delta \equiv \int_\Delta^\infty dP(\Delta')/ \int_0^\infty dP(\Delta')$, where $P(\Delta)$ is the distribution in Figure 8. Jets were required to have $|\eta| \geq 0.5$.

$$\left(\sum_i E_{Ti}\right)^2 \equiv \left(E_{t1} + E_{t2}\right)^2$$

$$= \left(E_1 \sin\theta_1 + E_2 \sin\theta_2\right)^2$$

$$= E_{T1}^2 + E_{T2}^2 + 2E_1E_2 \sin\theta_1 \sin\theta_2. \tag{53}$$

If we form the difference of the two expressions, we get

$$\left(E^2 - p_z^2\right) - \left(\sum_i E_{Ti}\right)^2 = E_1E_2 \sin^2\delta\theta,$$

where $\delta\theta \equiv \theta_1 - \theta_2$. We see that this difference is *always* positive, which means that using Eq. (48) underestimates the true E_T of a jet.

Again, we form the quantity

$$\Delta \equiv 1 - \frac{\sum_i E_{Ti}}{E_T} \tag{54}$$

which shows the fractional "error" in using Eq. (48) for the transverse energy, as opposed to Eqs. (4) and (36) for the "true" E_T. Figure 10 shows the distribution in Δ as so defined. As can be seen in the figure, the two different definitions of transverse energy give similar results. Differences are not large, and, in fact, Eq. (48) gives a smaller "error" than one obtains when using Eq. (49).
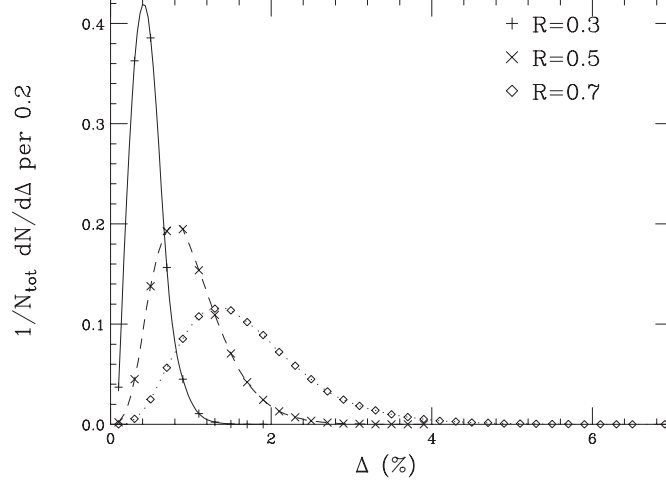
2.6. *The Mass of a Jet*

Fig. 10. Same as Figure 8, E_T defined using Eq. (48).

The mass of a jet can be calculated from its transverse momentum and energy using Eqs. (37) and (39):

$$
\begin{aligned}
M_{jet}^2 &\equiv E_{jet}^2 - p_{jet}^2 \\
&\equiv E_{Tjet}^2 - p_{Tjet}^2 \\
&= (E_{Tjet} - p_{Tjet})(E_{Tjet} + p_{Tjet})
\end{aligned}
\tag{55}
$$

Note that in the above equation, we formed the mass by using either $E^2 - p^2$ or $E_T^2 - p_T^2$. One should not confuse the mass of the jet as defined by $E_T^2 - p_T^2$ with what we have previously described as the "transverse mass". In fact, the transverse mass is only defined when dealing with 2 (or more) 4-vectors. A jet does not have a transverse mass.

In the limit when the jet energy gets large, the jet narrows – $\delta\phi_i \to 0$ and $\delta\eta_i \to 0$. We expand Eq. (37) for small $\delta\phi_i$ and Eq. (39) for small $\delta\eta_i$, yielding

$$
p_{Tjet} \to \sum E_{Ti}\left(1 - \frac{\delta\phi_i^2}{2}\right)
\tag{56}
$$

and

$$
E_{Tjet} \to \sum E_{Ti}\left(1 + \frac{\delta\eta_i^2}{2}\right).
\tag{57}
$$

Calculating the difference and sum between E_{Tjet} and p_{Tjet}, we have

$$
E_{Tjet} - p_{Tjet} = \frac{1}{2}\sum E_{Ti}(\delta\eta_i^2 + \delta\phi_i^2)
$$

$$E_{Tjet} + p_{Tjet} \quad = \quad \frac{1}{2} \sum E_{Ti} (4 + \delta\eta_i^2 - \delta\phi_i^2)$$

$$\simeq \quad 2 \sum E_{Ti} \tag{58}$$

where we have ignored the terms in $\delta\eta_i$ and $\delta\phi_i$ in the second equation. Inserting these relations into Eq. (55) gives

$$M_{jet}^2 = \sum E_{Ti} \sum E_{Ti} (\delta\eta_i^2 + \delta\phi_i^2) \tag{59}$$

Now we proceed to the small angle (thin jet) limit for large-E_T jets. As in the sections above, we can use the approximation $E_{Tjet} \simeq \sum E_{Ti}$, and combine with Eq. (42) to obtain the relation for the invariant mass of the jet as

$$M_{jet} \simeq \sigma_R \cdot E_{Tjet}. \tag{60}$$

This equation confirms what we know intuitively about the invariant mass of a multiparticle system, namely that the mass of the system is "generated by" the angles between the (approximately zero mass) particles.

Figure 11 shows the normalized distribution in mass (M_{jet}) for jets that were reconstructed with cone cutoffs of 0.3, 0.5, and 0.7. The distributions broaden as the cutoff increases due to inclusion of more towers further away from the jet center.
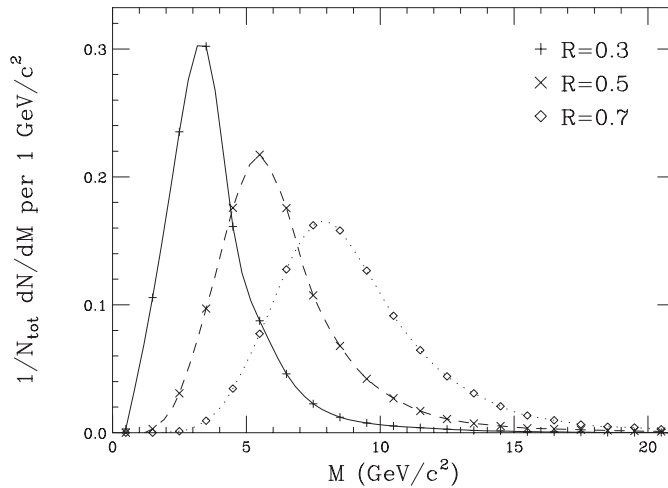

Fig. 11. Mass distribution for jets of different cone size.

In Figure 12 we plot the ratio $\sigma_R \cdot E_{Tjet}/M_{jet}$, on an event by event basis. These distributions show that the ratio is well within the few percent level of unity for all jet cones (note the vertical log scale used).
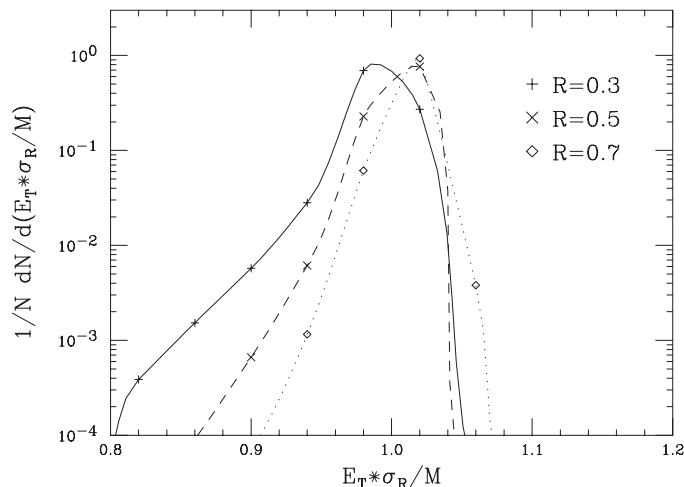
2.7. *Jet Merging*

Fig. 12. The distribution in the ratio $\sigma_R \cdot E_{Tjet}/M_{jet}$ for different cone sizes.

The merging of two jets is usually reflected in the value of σ_R, and, of course, in the size of the elements of the shape matrix. To study merging, we have used data from DØ, paying particular attention to whether there is evidence of any merging or splitting of jets as controlled by the jet algorithm parameters (see section). These data constitute our samples as described in the appendices.

Figure 13 shows the normalized distributions in σ_R for merged and not merged jets using our Sample 1, for $R = 0.3$, 0.5, and 0.7 cone sizes. We see a marked increase in the width of the merged jets for all cone cutoffs. (This sample is somewhat biased by the requirement that, after merging, there must be 2 and only 2 jets for all three defining cone sizes.)

Figure 14 shows the normalized distributions in σ_R using jets with cone cutoffs of 0.5 and 0.7, for events from Sample 2 (Appendix B). This sample was chosen to maximize the probability of collecting merged jets (unlike Sample 1, which was chosen to maximize the probability of collecting unmerged jets). The crosses and the dots are, respectively, σ_R spectra for the merged and unmerged jets respectively of Figure 13. It should be understood that each jet with $R = 0.7$ (0.5) in Sample 2 is required to be reduced to 2 jets of $R = 0.5$ (0.3). Figure 14 shows that σ_R correlates well, on average, with whether or not a jet is the result of a merging. We can therefore use the distributions from Figure 14 to construct a likelihood for a jet being from a merged or unmerged sample. Figure 15 shows the ratio of the probability distributions for non-merged and merged jets versus σ_R for cones of 0.3, 0.5, and 0.7. The points indicate the values of σ_R for relative likelihoods of 1 (equal probability of being from either distribution); these are listed in Table 2.

Finally, we investigate the shape of jets via correlations in σ_η/σ_ϕ with respect to merging. If jets were circular in $\eta\phi$ space, we would expect that the quantity $\Delta\sigma \equiv \sqrt{\sigma_{\eta\eta}} - \sqrt{\sigma_{\phi\phi}}$ would be Gaussian-distributed around 0. If jets result from merging, then we expect the shape of the jet in $\eta\phi$ space to become elongated, forming an ellipse, and the quantity $\Delta\sigma$ would deviate from 0. We use the normalized quantity
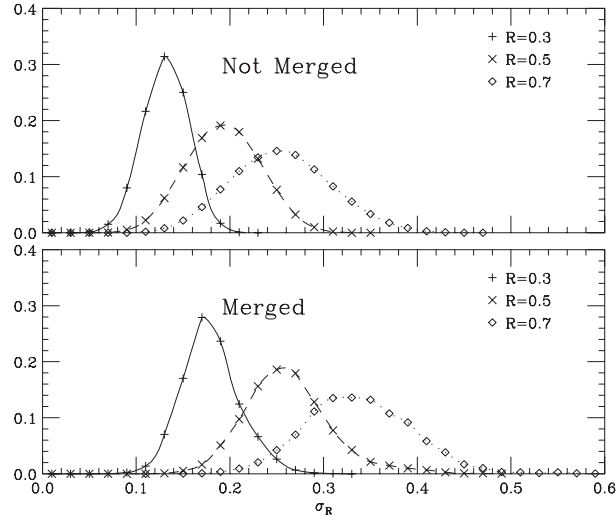
Fig. 13. Normalized distributions in σ_R for jets that were merged (bottom) and those that have *not* been merged (top), for different cone sizes.
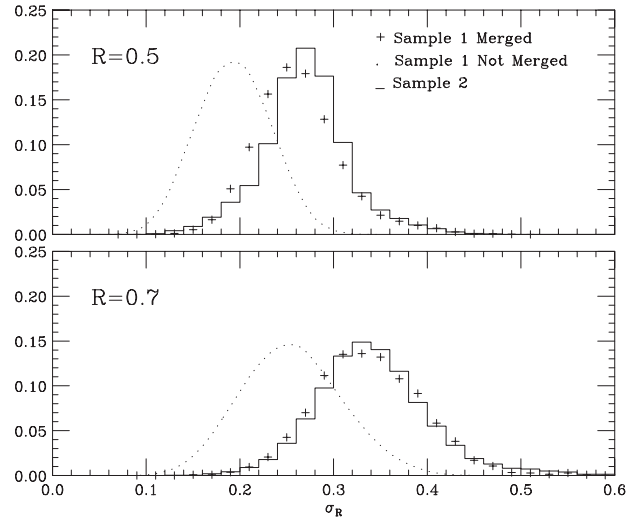

Fig. 14. Normalized distributions of σ_R for single jets that are associated with 2 jets found by way of a smaller cone cutoff (see text).
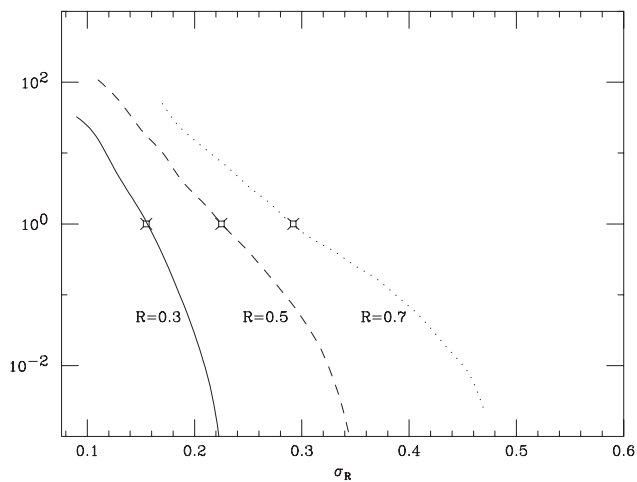
Fig. 15. Relative likelihood for a jet being non-merged to a jet being merged as a function of σ_R, for three jet cones. Relative likelihoods of 1 are indicated by the points on the curves.

Table 2. Value for σ_R corresponding to a a relative likelihood of unity for jets to be from non-merged or merged distributions.

R	$\sigma_R(1)$
0.3	0.155
0.5	0.224
0.7	0.292

$$\delta_{\eta\phi} \equiv \frac{\sigma_{\eta\eta} - \sigma_{\phi\phi}}{\sigma_{\eta\eta} + \sigma_{\phi\phi}}$$

which, to first order, should be independent of the cone size for symmetric jets. This is indeed observed in Figure 16, where we show $\delta_{\eta\phi}$ for jets from Sample 1 with cones 0.3, 0.5, and 0.7. Figure 17 shows the same distribution from Sample 2.
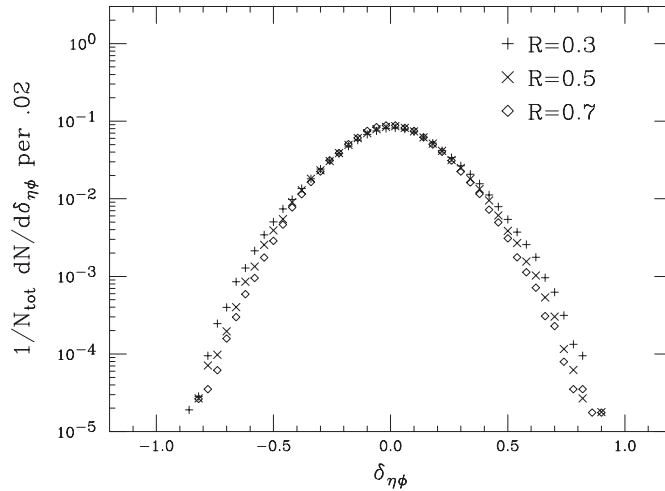

Fig. 16. The distribution in $\delta_{\eta\phi} \equiv \frac{\sigma_{\eta\eta} - \sigma_{\phi\phi}}{\sigma_{\eta\eta} + \sigma_{\phi\phi}}$ using unmerged jets with cone cutoffs of 0.3, 0.5, and 0.7 from Sample 1.

As demonstrated above, these jets are broader than "pure" unmerged jets, however Figure 17 also shows that the broadening of σ_R can be associated with a broadening in *either* δ_η or δ_ϕ.

2.8. *Summary*

The above sections are intended to give a pedagogic description of jets, towards an understanding which is self consistent and illuminating. For the particle physicist, the next step is to learn more about the physics of jets, *i.e.* characteristics of jet production, which in turn will allow understanding of the fundamental processes underlying the physics of interest.

Appendix A - Events Used in Sample 1

A sample of events was used with the following requirements:

(i) Pathologies (Main Ring splash, cosmic rays, *etc.*) were eliminated.
(ii) The position of the collision vertex was required be within ±60cm of the longitudinal center of the DØ detector.
(iii) Each event had to have 2 and only 2 reconstructed jets for cones of 0.3, 0.5, and 0.7, with none of the jets formed from merging of two or more jets of lower
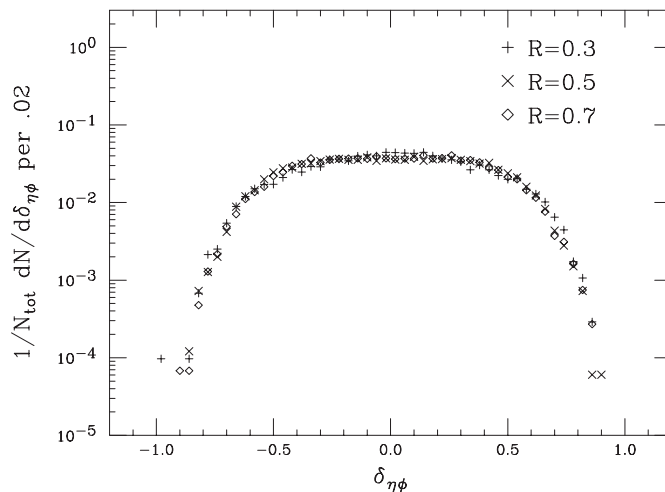
Fig. 17. The distribution in $\delta_{\eta\phi} \equiv \frac{\sigma_{\eta\eta}-\sigma_{\phi\phi}}{\sigma_{\eta\eta}+\sigma_{\phi\phi}}$ using merged jets with cone cutoffs of 0.3, 0.5, and 0.7 from Sample 2.

  transverse energy (by merging, we mean that there was no explicit merging by the jet cone algorithm as described above).
(iv) All τ, electron, and photon candidates are rejected by requiring a minimum for cluster $\sigma_{\eta\eta}$ and $\sigma_{\phi\phi}$, depending on the cone size. The cutoffs used were $(0.025)^2$, $(0.040)^2$, and $(0.060)^2$ for cones of 0.3, 0.5, and 0.7, respectively.

These requirements were chosen to maximize the probability of selecting events with only 2 jets at tree level. Nevertheless, we cannot exclude the presence of events with 3 or more jets, where jets were merged two at a time a priori due to their extreme closeness in $\eta\phi$ space. Such contamination should be small. In addition, there are (probably small) biases due to *e.g.* trigger thresholds (since the DØ jet trigger starts with a single trigger tower threshold, thinner jets are more likely than fat jets to pass the trigger requirement) and primary vertex cuts (item *ii* above is not a very restrictive cut). However, the results presented here are intended to be purely qualitative in nature.

Appendix B - Events selected for Sample 2

These events were chosen to have a sample of merged jets. Events were required to satisfy the same criteria **1** and **2** used to define Sample 1, but only events that had 3 jets reconstructed with a cone size of 0.3, and 2 jets with a cone size of 0.5 or 0.7 were analyzed, guaranteeing the presence of two well separated clusters of energy within a jet. About 6.5% of all events were classified in this manner.

1. V. Barger and R. Phillips, *Collider Physics* (Addison-Wesley, Reading, MA, 1987).
2. D. Perkins, *Introduction to High Energy Physics, 3rd Edition* (Addison-Wesley, Reading, MA, 1987), pp. 354–356.

3. H. Bøggild and T. Ferbel, "Inclusive Reactions", *Annual Review of Nuclear and Particle Science* **24**, 451 (1974).

4. DØ Collaboration, S. Abachi *et al.*, *NIM* **A338**, 185 (1984).

5. As of this submission, the most precise published value of the W mass is $80.41 \pm 0.09 GeV/c^2$ from a combination of DØ CDF, and UA2 data. By adding the most recent LEP2 data, the W mass changes to $80.40 \pm 0.08 GeV/c^2$. These results were presented by D. Wood at the June 1997 Hadron Collider Physics conference at Stony Brook. Proceedings for this conference will be available online at http://sbhep1.physics.sunysb.edu/ hadrons/proceedings.html.

6. D. Gross and F. Wilczek, *Phys. Rev. Lett.* **30**, 1343 (1974).

7. H. Politzer, *Phys. Rev. Lett.* **30**, 1346 (1974).

8. J. Huth and M. Mangano, "QCD Tests in Proton–Antiproton Collisions", *Ann. Rev. Nucl. Part. Sci.* **43** 585, (1993).

9. S. Bethke, in *Proceedings of the XXIII International Conference on High Energy Physics, Berkeley, 1986*, ed. S. Loken, (World Scientific, 1987), Volume II, pp. 1086–1087.

10. G. Hanson, in *Proceedings XIII Rencontre de Moriond, 1978*, ed. J. Tran Thanh Van, Vol. II, p. 15.

11. PLUTO Collaboration, Ch. Berger *et al.*, *Phys. Lett.* **78B** 176 (1978).

12. G. Thompson, in *Proceedings of the XXIII International Conference on High Energy Physics, Berkeley, 1986*, ed. S. Loken, (World Scientific, 1987), Vol II, p. 1153.

13. Herbert Goldstein, *CLASSICAL MECHANICS (2nd Edition)*, (Addison-Wesley, 1980) pp. 146–147. The Euler transformation used here is given by equation 4-46 with the condition $\psi = 0$ and $\phi \rightarrow \phi + \pi/2$.

14. UA1 Collaboration, Arnison, G. *et al.*, *Phys. Lett.* **123B**, 115 (1983), **132B**, 214 (1983), and **172B**, 461 (1986).

15. CDF Collaboration, F. Abe *et al.*, *Phys. Rev. Lett.* **62**, 613 (1989), **69**, 2898 (1992), and perhaps most importantly *Phys. Rev.* **D45**, 1448 (1992).

16. DØ Collaboration, S. Abachi *et al.*, *Phys. Rev.* **D52** 4877 (1995).

17. UA2 Collaboration, M. Banner *et al.*, *Phys. Lett.* **118B**, 203 (1982).